ADVANCED FUNCTIONAL MATERIALS
www.afm-journal.de

Over 100 cd A^{-1} Efficient Quantum Dot Light-Emitting Diodes with Inverted Tandem Structure

*Heng Zhang, Xiaowei Sun, and Shuming Chen**

Quantum dot light-emitting diodes (QLEDs) with tandem structure are promising candidates for future displays because of their advantages of pure emission color, long lifetime, high brightness, and high efficiency. To obtain efficient QLEDs, a solution-processable interconnecting layer (ICL) based on poly(3, 4-ethylenedioxythiophene)/polystyrene sulfonate/ZnMgO is developed. With the proposed ICL, all-solution-processed, inverted, tandem QLEDs are demonstrated with high current efficiency (CE) of 57.06 cd A^{-1} and external quantum efficiency (EQE) of 13.65%. By further optimizing the fabrication processes and using a hybrid deposition technique, the resultant tandem QLEDs exhibit a very high CE over 100 cd A^{-1} and an impressive EQE over 23%, which are the highest values ever reported and are comparable with those of the state-of-the-art phosphorescent organic LEDs. Moreover, the efficiency roll-off, a notorious phenomenon in phosphorescent LEDs, is significantly reduced in the developed QLEDs. For example, even at a very high brightness over 200 000 cd m^{-2}, the tandem QLEDs can still maintain a high CE of 96.47 cd A^{-1} and an EQE of 22.62%. The proposed ICL and the developed fabrication methods allow for realization of very efficient tandem QLEDs for next generation display and lighting applications.

1. Introduction

Recently, light-emitting diodes (LEDs) based on colloidal quantum-dots (QDs) have been intensively investigated because of their potential applications in next generation displays owing to their unique features such as self-emitting, tunable emission spectra, pure emission color, easy fabrication, excellent flexibility, and high photostability.[1–8] Since the first quantum dot light-emitting diodes (QLEDs) have been demonstrated, the device performances have been improved greatly with the rapid development of QD materials and device architectures.[2,9–11] For example, red QLEDs with external quantum efficiency (EQE) of 20.5% have been reported by Peng and co-workers.[2] However, even though the researchers are struggling to optimize the QD materials and the device structures, the performances of QLEDs are still much lower than those of the state-of-the-art organic light-emitting diodes (OLEDs),[2,12–16] especially the green and the blue QLEDs.[13–16] Therefore, it is necessary to develop a new strategy for further boosting the performances, especially the efficiency and the lifetime of QLEDs for practical applications.

Tandem structures which use interconnecting layer (ICL) to connect two or more light-emitting units in series offer the advantages of high current efficiency (CE) and long operational lifetime and thus are widely adopted in OLED display and lighting.[17,18,24] Because of the similar properties of OLEDs and QLEDs, it is a feasible and promising way to improve the efficiency/lifetime of QLEDs by using tandem structures. However, it is more challenging to develop tandem QLEDs. For one thing, QDs are usually deposited by solution processes, whereas most efficient ICLs based on small molecules are easily damaged by the solvents during deposition of the top QD layers. For another, tandem devices usually consist of many functional layers, whereas it is extremely difficult to solution-deposit all functional layers without causing damages. Thus, all-solution-processed tandem QLEDs have rarely been reported. Only Jang and co-workers demonstrated tandem QLEDs, but the performances are very poor, which is likely due to the inefficient ICL and the poor morphologies of the deposited films.[19] Previously, we have proposed a novel deposition process to realize all-solution-processed, multilayered, inverted QLEDs[20] and to prevent the thermally evaporated ICL from damaging by the solution processes, we have developed a hybrid tandem structure, which integrates QLED and OLED in series.[21] Based on our previous work, we further develop all-solution-processed tandem QLEDs in this report.

To address the challenges of tandem QLEDs aforementioned, we first develop a new solution-processed ICL based on a P (Positive)-N (Negative) heterojunction. Poly(3, 4-ethylenedioxythiophene)/polystyrene sulfonate (PEDOT:PSS) is adopted as the p-type material because of its high conductivity and high work function. ZnO nanoparticles are ideal n-type materials because of their high electron mobility and high optical transparency.[22,23] However, because of the acidic nature of PEDOT:PSS, reactions/corrosions between PEDOT:PSS and ZnO may occur, leading to the low performance of the ICL.[24] To prevent the possible reactions between ZnO and PEDOT:PSS, Kido and co-workers have proposed using a neutralized PEDOT:PSS and successfully obtained an solution-processed ICL for tandem OLEDs.[24] In this work,

H. Zhang, Prof. X. Sun, Prof. S. Chen
Department of Electrical and Electronic Engineering
Southern University of Science and Technology
Shenzhen 518055, P. R. China
E-mail: chen.sm@sustc.edu.cn

DOI: 10.1002/adfm.201700610

we find that by doping Mg into ZnO, the resultant ZnMgO alloy nanoparticles can work with PEDOT:PSS perfectly, and consequently, the developed ICL based on PEDOT:PSS/ZnMgO heterojunction can efficiently generate holes and electrons under reverse bias. With the proposed ICL, all-solution-processed tandem QLEDs are successfully demonstrated with high CE of 57.06 cd A^{-1} and EQE of 13.65%. By further optimizing the fabrication processes and using a hybrid deposition technique, the resultant tandem QLEDs exhibit a very high CE over 100 cd A^{-1} and an impressive EQE over 23.68%, which, to the best of our knowledge, are the highest values ever reported. The efficiencies of our demonstrated QLEDs are comparable with those of the state-of-the-art phosphorescent OLEDs, whereas the color saturation is significantly higher than that of OLEDs. Moreover, the efficiency roll-off, a notorious phenomenon in phosphorescent OLEDs, is significantly reduced in our developed QLEDs. The proposed ICL and the developed fabrication methods allow for realization of very efficient tandem QLEDs for next generation displays and lighting applications.

2. Results and Discussion

Figure 1 shows the structures, the cross-sectional transmission electron microscopic (TEM) images, and the energy band diagrams of the tandem QLEDs. Inverted structures were adopted because they allow QLEDs to integrate with high performance n-type metal oxide transistors. Two inverted sub-QLEDs with identical structure were serially connected via the ICL based on PEDOT:PSS/ZnMgO heterojunction. PEDOT:PSS is widely used as hole injection material and ZnMgO is an ideal electron injection and transport material for QLEDs.[25] Because of the high carrier mobility and the well-aligned energy levels, the ICL can efficiently generate and inject carriers to the sub-QLEDs, as schematically illustrated in Figure 1c. The tandem QLEDs consist of ten functional layers in total and all functional layers except the electrodes were deposited by spin-casting method. To investigate whether all functional layers still survive after solution-processing for so many times, the cross-sections of the devices were examined using TEM. As shown in Figure 1b, all functional layers can be clearly observed, confirming the existence of the functional layers even after processing for many times.

One of the challenges of making all-solution-processed QLEDs is that the functional layers are easily damaged by the solvents. Even the functional layers can survive after solution processing, whether they are damaged by the solvents remains a question. For example, for the inverted QLEDs with structure glass/indium tin oxide (ITO)/ZnMgO/QDs/poly(9-vinlycarbazole) (PVK)/PEDOT:PSS/Al, the QD light-emitting layer is easily damaged by the solvents of PVK, leading to the poor performances of the devices. Therefore, inverted QLEDs fabricated by all-solution-process have rarely been reported.[20] To make damage-free QLEDs, we have adopted a novel fabrication method as we previously proposed.[20] To examine whether

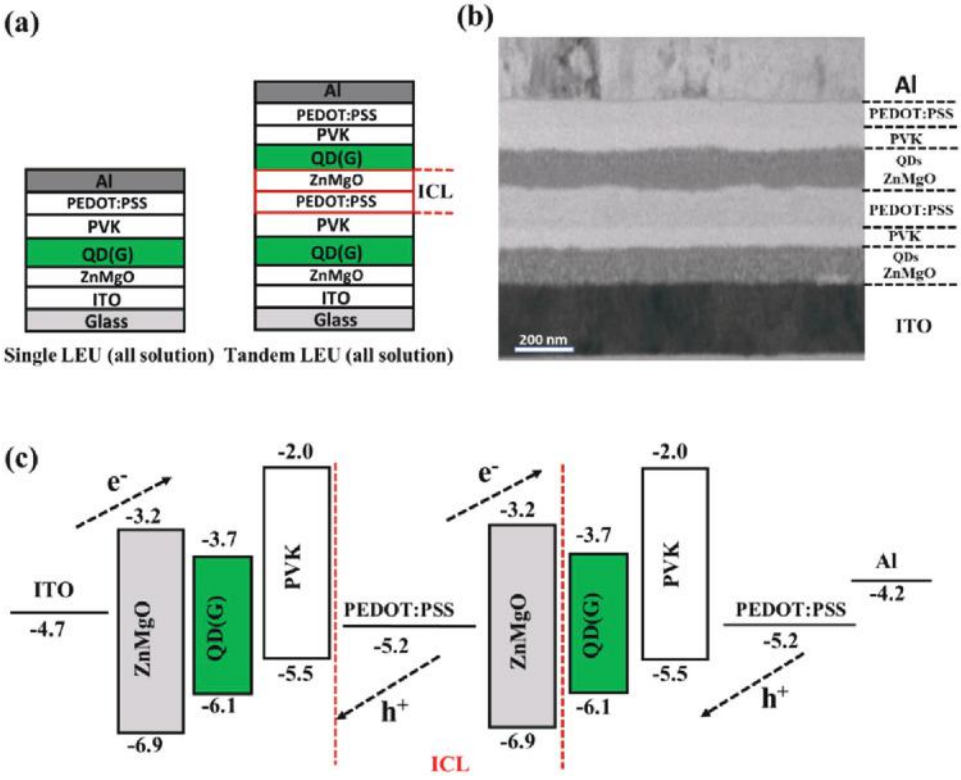

Figure 1. a) Schematic device structure of all-solution-processed single QLEDs and tandem QLEDs. b) Cross-sectional TEM image of all-solution-processed inverted tandem QLEDs. c) Energy band diagram of the all-solution-processed tandem QLEDs. A new ICL based on PEDOT:PSS/ZnMgO is used to connect the two individual QLEDs.

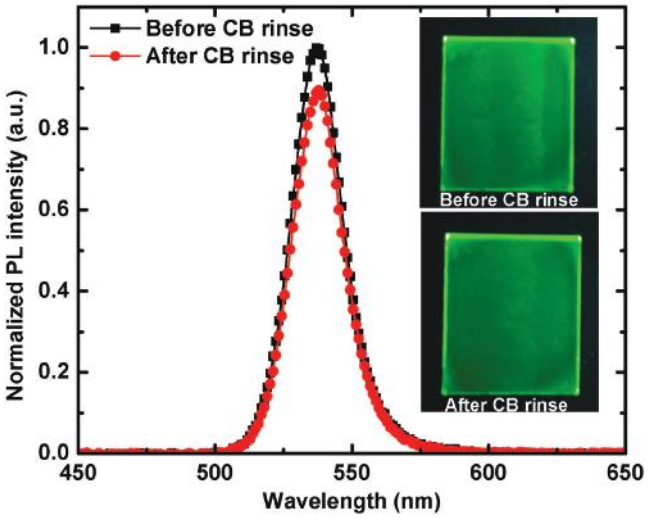

Figure 2. PL spectra of the QD layer coated on ZnMgO before and after CB rinsing. The inset shows the photographs of the samples before and after CB rinsing under the illumination of ultraviolet light source.

the QD layer was damaged by the solvent (chlorobenzene, CB) of PVK, the photoluminescence (PL) intensity of the QD layer coated on ZnMgO layer before and after CB rinsing were measured. As shown in **Figure 2**, the PL intensity of the QD layer after CB rinsing is slightly lower than that without CB rinsing. Inset of Figure 2 shows the PL images of the samples before and after CB rinsing, and no obvious damages can be observed for the samples rinsed by CB. These results confirm that by using our developed deposition processes, the QD layer almost is not damaged by the solvent of PVK.

Another challenge is that it is difficult to uniformly deposit the aqueous PEDOT:PSS onto the PVK, which is hydrophobic in nature. To address this issue, a small amount of iso-propanol (IPA) was added into the PEDOT:PSS. With IPA additive, the wettability of PEDOT:PSS on PVK is significantly enhanced and thus uniform PEDOT:PSS layer can be obtained.[20]

Last but not least, the ICL should be able to efficiently generate and inject charge carriers to the sub-QLEDs under electrical driving. To examine the charge generation ability of the proposed ICL, the ICL-only devices with structure glass/ITO/PEDOT:PSS/ZnMgO/Al were fabricated and their current density–voltage (*J*–*V*) characteristics were measured. The working processes of the ICL under electrical driving are schematically shown in **Figure 3**a,b. When the ICL is forward biased, holes and electrons are injected from their corresponding electrode and subsequently recombined at the interface between PEDOT:PSS and ZnMgO. On the contrary, when the ICL is reversely biased, holes and electrons are generated and then drifted to the respective electrode by the reverse electric field. Figure 3c shows the *J*–*V* characteristics of the ICL-only devices under forward and reverse bias. The current density increases rapidly as the driving voltage increases. The forward current is attributed to the charges injected from the electrodes, whereas the reverse current is stem from the charge carriers that are generated from the ICL. It is obvious that the reverse current is nearly equal to the forward current, which indicates that the charge generation is as efficient as the charge injection. The charge

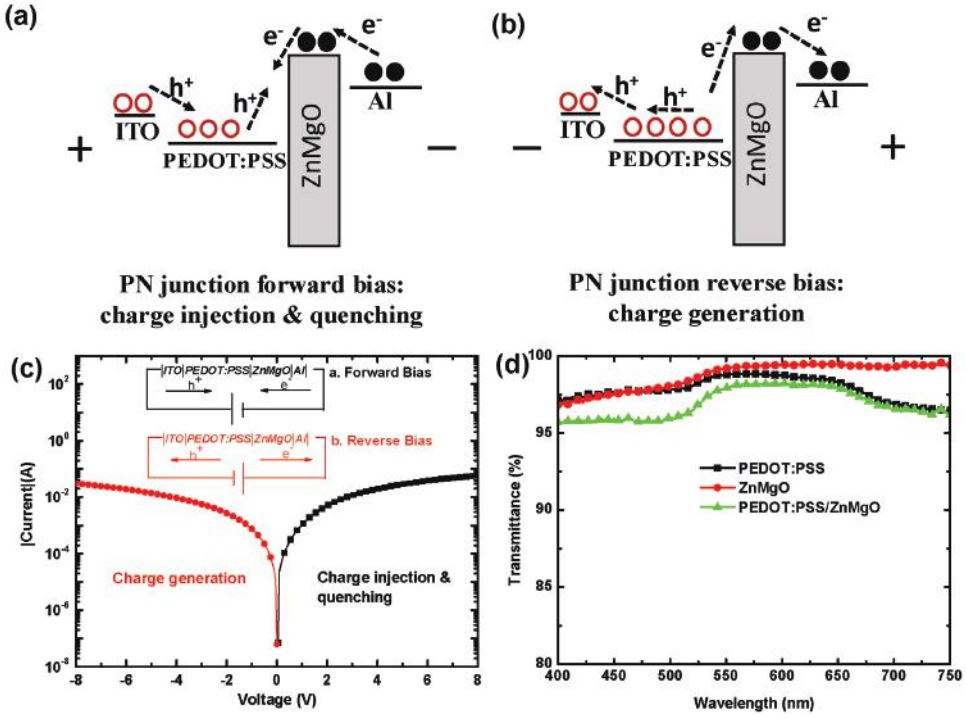

Figure 3. a) PN junction under forward bias, charge carriers are injected and subsequently quenched in the ICL. b) PN junction under reverse bias, charge carriers are generated from the ICL. c) *J*–*V* characteristics of the ICL-only devices. Inset: Equivalent circuit of the ICL-Only devices under forward and reverse bias. d) Transmittances of the PEDOT:PSS, the ZnMgO and the ICL.

injection, including holes injected from ITO to PEDOT:PSS and electrons injected from Al to ZnMgO, is very efficient because of the well-aligned energy levels and the high carrier mobility of the materials adopted. Thus, one can conclude that the charge generation is also very efficient, which is crucial to efficient tandem devices. Because of the efficient charge carrier injection, the excitons are generated by direct carrier injection instead of Förster energy transfer from adjacent charge transport layer. The transmittances of the PEDOT:PSS, ZnMgO and ICL layer were also investigated and shown in Figure 3d. The proposed ICL exhibits a high transmittance over 95% in the visible spectral range, which is beneficial for light outcoupling.

The excellent charge generation capability and the high transparency of the ICL encourage us to further explore its application in tandem QLEDs. All-solution-processed tandem devices with structure ITO/ZnMgO (40 nm)/QDs (18 nm)/PVK (30 nm)/PEDOT:PSS (35 nm)/ZnMgO (40 nm)/QDs (18 nm)/PVK (30 nm)/PEDOT:PSS (35 nm)/Al (100 nm) were fabricated. Single QLEDs were also fabricated for comparison. **Figure 4**a shows the normalized electroluminescent (EL) spectra of the devices. Both single and tandem devices exhibit identical pure green emission with central wavelength of 538 nm and full width at half maximum (FWHM) of 23 nm. Figure 4b shows the photos of the tandem devices operated under different current levels. Very bright and uniform emission can be observed. Figure 4c,d compares the *J*–*V* and luminance–voltage (*L*–*V*) characteristics of the devices. At a certain current level, the driving voltage of the tandem QLEDs is nearly twofold higher than that of single QLEDs, which is reasonable since the tandem devices consist of two single QLEDs connected in series. The turn on voltage for 1 cd m^{-2} of the tandem QLEDs is 7.3 V, which is nearly doubled that (3.7 V) of the single devices. No voltage is dropped on the ICL, indicating that the ICL can efficiently generate and inject charge carriers to the top and the bottom sub-QLEDs. The CE and EQE of the devices are compared in Figure 4e,f. The tandem devices exhibit a high CE of 57.06 cd A^{-1} and an EQE of 13.65 cd A^{-1}, which are nearly twofold higher than 29.68 cd A^{-1} and 7% for the single devices. The detailed device performances are summarized in **Table 1**. To test the reproducibility, ten devices from different batches were fabricated and their efficiencies are summarized in Figure S1 (Supporting Information). The results indicate our developed fabrication processes and the performances of the tandem QLEDs are highly repeatable.

Though solution deposition offers the advantage of low cost, the qualities such as the uniformity, the morphology of the deposited films are relatively poor, especially when the films are subjected to multiple solvent treatments. **Figure 5** shows the evolution of the morphologies of the tandem devices. Initially, the solution-deposited films are quite smooth with a low surface roughness of 0.438 nm. However, after solution processing for many times, the surface roughness is increased to 2.912 nm, as shown in Figure 5e–h. The morphology of the top PEDOT:PSS layer is the poorest, as nonuniform spots can be observed from the microscopic image shown in Figure 5d. The poor morphology of the top PEDOT:PSS can also be verified by its high surface roughness of 2.912 nm. The bad morphology of the top PEDOT:PSS layer remarkably influences its contact with Al anode and can likely increase the contact resistance, reduce the charge balance, and decrease the power efficiency of the devices.

In addition, only a few polymer materials are compatible with the solution processes, whereas most small-molecular charge transport materials cannot be deposited by solution methods, which limits the optimization of device architectures. Therefore, to further improve the performances of devices, a hybrid deposition process is adopted. The bottom sub-QLEDs were fabricated by solution processes, whereas to improve the morphologies and enhance the charge injection,

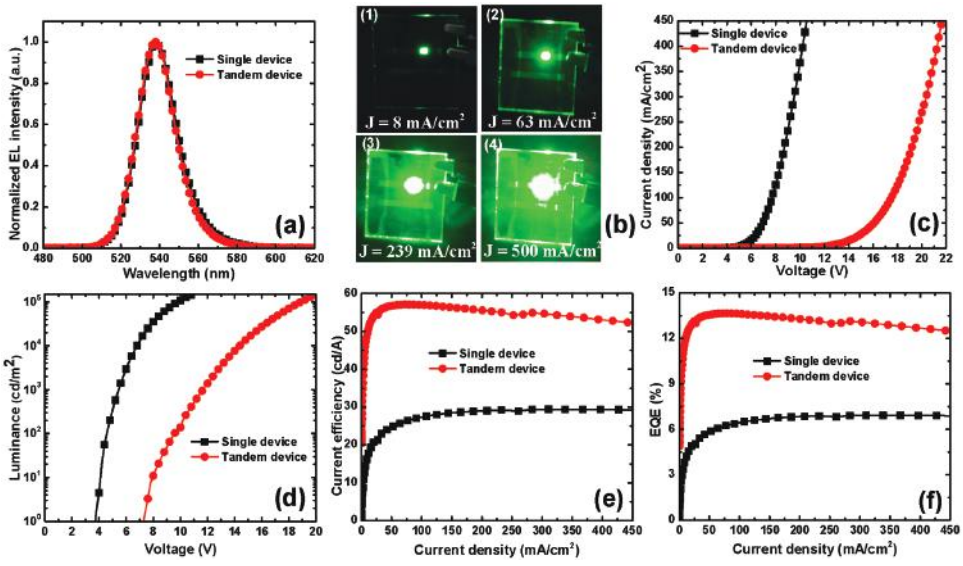

Figure 4. a) Normalized EL spectra of the single and the tandem devices. b) The photos of the devices with driving current density of 8, 63, 239, and 500 mA cm^{-2}, respectively. c) *J*–*V* characteristics, d) *L*–*V* characteristics, e) CE-J characteristics, and f) EQE-J characteristics of the all-solution-processed single and tandem QLEDs.

Table 1. The device performances of all-solution-processed single and tandem QLEDs.

Device	V_{on}	CE [cd A^{-1}]		EQE (%)		PE [lm W^{-1}]	
		500/5000/50000 [cd m^{-2}]	Max	500/5000/50000 [cd m^{-2}]	Max	500/5000/50000 [cd m^{-2}]	Max
Single device	3.7	12.45/20.83/28.97	29.68	2.94/4.91/6.83	7.00	7.52/10.55/10.83	11.33
Tandem device	7.3	31.54/50.48/56.97	57.06	7.54/12.07/13.63	13.65	9.00/11.65/10.28	11.72

the hole injection/transport layers (HTL) of the top sub-QLEDs were deposited by thermally vacuum evaporation. Small molecular multilayered 4,4′,4″-tris(carbazol-9-yl)triphenylamine (TcTa)/*N*,*N*′-di(naphthalene-1-yl)-*N*,*N*′-bis(phenyl)-benzidine (NPB)/dipyrazino [2,3-f:2′,3′-h] quinoxaline-2,3,6,7,10,11-hexacarbonitrile (HATCN) was adopted to substitute the problematic PVK/PEDOT:PSS as efficient HTL for the top sub-QLEDs. Because of the improved morphologies and the well-aligned energy levels, the devices with evaporated HTL are expected to exhibit improved performance. To verify our assertions, tandem QLEDs with structure glass/ITO/ZnMgO (40 nm)/QDs (18 nm)/PVK (30 nm)/PEDOT:PSS (35 nm)/ZnMgO (40 nm)/QDs (18 nm)/TcTa (25 nm)/NPB (20 nm)/HATCN (10 nm)/Al (100 nm) were fabricated. The bottom and the top sub-QLEDs were also fabricated for comparison. The structures, the cross-sectional TEM images, and the energy band diagrams of the devices are shown in Figure S2 (Supporting Information).

The normalized EL spectra of the single and the tandem devices are depicted in Figure S3 (Supporting Information). All devices exhibit identical EL spectra with very pure green emission. **Figure 6**a,b shows the *J*–*V* and *L*–*V* characteristics of the devices. The top sub-QLEDs with evaporated HTL exhibit superior performances to those of the bottom sub-QLEDs. For example, the turn on voltage of the top sub-QLEDs is lower than that of the bottom sub-QLEDs. Also, the top sub-QLEDs exhibit a CE of 35.7 cd A^{-1}, which is relatively higher than 29.68 cd A^{-1} for the bottom sub-QLEDs. The improved performances are likely due to the improved morphologies and the enhanced hole injection. Figure 6c,d shows the efficiency of the devices. Because of the improved efficiency of the top sub-QLEDs, the efficiency of the tandem QLEDs is further increased to 71 cd A^{-1} (corresponding to an EQE of 16.76%). Benefit by the efficient ICL, the CE of the tandem QLEDs is even higher than the sum of 35.7 and 29.68 cd A^{-1} for the top and the bottom sub-QLEDs, respectively. In addition, the power efficiency of the tandem QLEDs is also higher than that of the single QLEDs, as shown in Figure S4 (Supporting Information). These results indicate that the charge generation and injection from the ICL to the sub-QLEDs are even more efficient than that from the electrodes.

To further boost the performances of the devices, a Ga-based liquid metal (EGaIn) was used to substitute Al as anode. We previously demonstrated with EGaIn electrode, vacuum-free-processed QLEDs can be obtained with superior performance.[26] The native oxide of EGaIn plays an important role in enhancing the performances of the devices. As shown in Figure 6a–d, with EGaIn electrode, tandem QLEDs exhibit a very high CE over 101 cd A^{-1} and an impressive EQE of 23.68%, which are about 1.42-fold higher than 71 cd A^{-1} and 16.76% for the devices with Al electrode. The improved performances

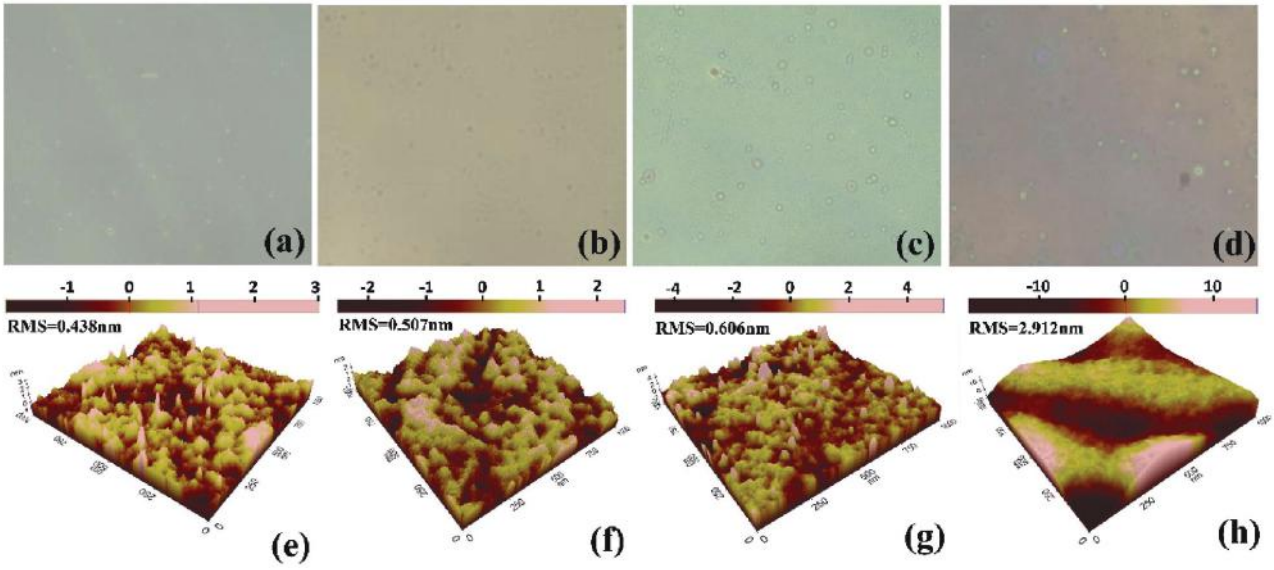

Figure 5. Optical microscopy and atomic force microscopy (AFM) images of the samples with structures: a) ITO/ZnMgO/QD/PVK, b) ITO/ZnMgO/QD/PVK/PEDOT:PSS, c) ITO/ZnMgO/QD/PVK/PEDOT:PSS/ZnMgO/QD/PVK, and d) ITO/ZnMgO/QD/PVK/PEDOT:PSS/ZnMgO/QD/PVK/PEDOT:PSS.

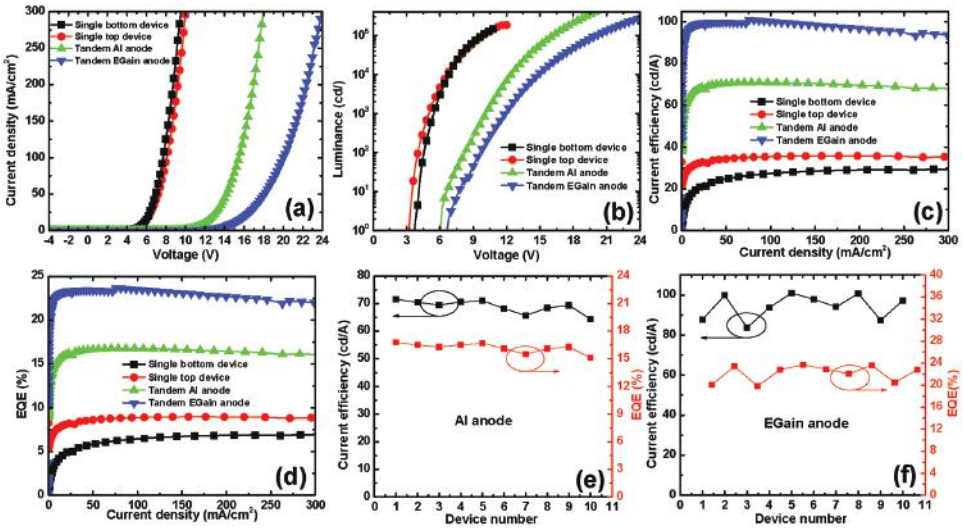

Figure 6. a) *J–V* characteristics, b) *L–V* characteristics, c) *C–J* characteristics, and d) *E–J* characteristics of the devices. (e) and (f) are the statistical device performances of the tandem devices with Al and EGaIn anode, respectively.

are likely due to the reduction of leakage current and more balance of charge injection. The detailed mechanisms will be reported elsewhere. Figure 6e,f summarizes the efficiencies of ten devices fabricated from different batches. The averaged efficiencies for the tandem QLEDs with Al and EGaIn electrode are 68.91 and 94.35 cd A^{-1} respectively. The results indicate that the performances of our demonstrated tandem QLEDs are highly repeatable. It should also be noted that the lifetime of our tandem QLEDs is expected to be significantly longer than that of the single QLEDs. This is because the current efficiency of the tandem devices is twofold higher than that of the single devices, and thus, at a certain luminance, the current required for the tandem devices is only one half of that required for the single devices. It is known that LEDs operated at small current can exhibit significantly prolonged lifetime. The detailed device performances are summarized in **Table 2**.

The performances of our developed tandem QLEDs outperform most of the reported devices,[15,22,26–35] and to the best of our knowledge, this is the first reported QLED with CE over 100 cd A^{-1}. **Figure 7** shows the evolution of the CE of conventional and inverted green QLEDs over the past 10 years. The efficiencies of our developed tandem QLEDs are the highest and are comparable with state-of-the-art phosphorescent OLEDs.[36–38] Besides, the color saturation of our tandem QLEDs is significantly higher than that of OLEDs. As shown in Figure S3 (Supporting Information), the tandem QLEDs exhibit very pure emission with an FWHM of 23 nm and commission internationale de L'Eclairage (CIE) coordinates of (0.2067, 0.7544), which is almost located at the edge of the color chart, whereas the FWHM of most OLEDs is larger than 60 nm and thus the color is far from saturated.[39] Moreover, the high efficiency of our tandem QLEDs can still be maintained even at a very high luminance, whereas the peak efficiency of most phosphorescent OLEDs is usually achieved at small luminance and it rolls off very quickly at high luminance/current density due to triplet–triplet annihilation.[40,41] For example, as shown in Figure 6c,d, even at a very high luminance over 200 000 cd m^{-2}, the tandem QLEDs can still exhibit a high CE of 96.47 cd A^{-1} and an EQE of 22.62%, which are also the highest values compared to those of phosphorescent OLEDs operated at such high luminance. Thus, the developed tandem QLEDs, here with high color saturation, high efficiency, and reduced efficiency roll-off, would be ideal candidates to bring QLEDs into next generation display and lighting market.

3. Conclusions

In summary, very efficient, inverted tandem QLEDs with CE over 100 cd A^{-1} have been developed in this contribution.

Table 2. The device performances of bottom sub-QLEDs, top sub-QLEDs, and tandem QLEDs.

Device	V_{on}	CE [cd A^{-1}]		EQE (%)		PE [lm W^{-1}]	
		500/5000/50000 (cd m^{-2})	Max	500/5000/50000 (cd m^{-2})	Max	500/5000/50000 (cd m^{-2})	Max
Single (bottom device)	3.7	12.45/20.83/28.97	29.68	2.94/4.91/6.83	7.00	7.52/10.55/10.83	11.33
Single (top device)	3.2	24.79/32.12/35.64	35.70	6.22/8.06/8.94	8.95	16.92/16.27/13.01	17.01
Tandem (Al anode)	6.1	47.72/62.91/70.93	71.00	11.27/14.85/16.75	16.76	15.61/17.03/15.05	17.03
Tandem (EGain anode)	6.3	72.45/93.95/99.78	101.00	16.99/22.03/23.39	23.68	19.96/20.49/16.49	20.93

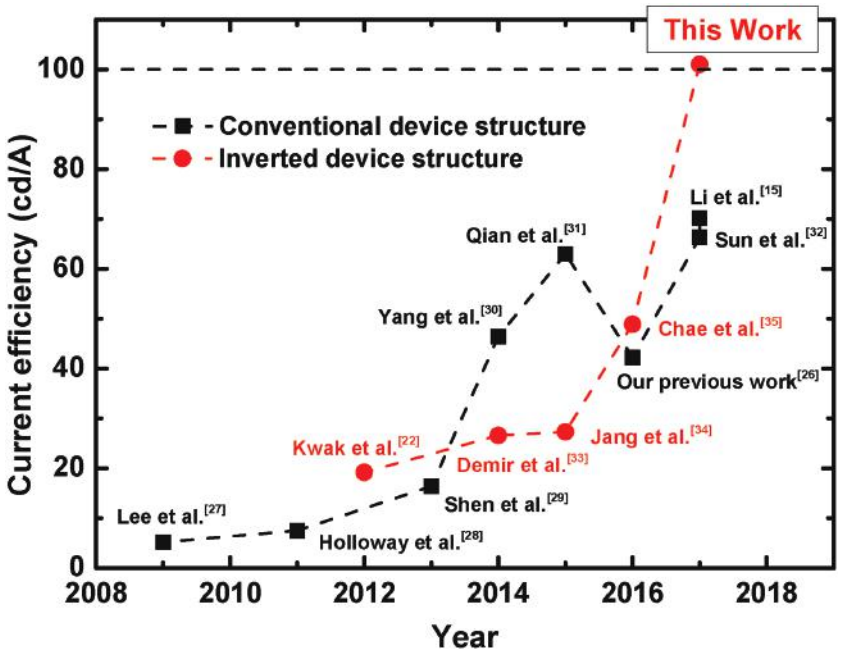

Figure 7. Evolution of the current efficiency of the conventional and inverted green QLEDs over the past 10 years. All data are based on Cd-based green QLEDs.

Such high efficiency has been achieved by (1) using a novel solution-deposition process to reduce the damage of QD light-emitting layers and to improve the uniformity of PEDOT:PSS layers; (2) developing a solution-processed ICL based on PEDOT:PSS/ZnMgO heterojunction, which can efficiently generate and inject charge carriers to the sub-QLEDs; (3) adopting a hybrid deposition process to improve the morphologies and charge injection efficiency of the HTL for the top sub-QLEDs; and (4) employing EGaIn-based liquid metal to further reduce the leakage current and improve the charge balance of the devices.

The efficiencies of the demonstrated tandem QLEDs outperform most of the reported QLEDs and are comparable with those of the state-of-the-art phosphorescent OLEDs. Our results demonstrate that it is a good strategy to boost the performances of the QLEDs by using proposed ICL and developed fabrication methods. Together with their high color saturation, reduced efficiency roll-off, and long operational lifetime, the tandem QLEDs are ideal candidates to bring QLEDs into next generation display and lighting market.

4. Experimental Section

Device Structures: All-solution-processed tandem QLEDs with structures of ITO/ZnMgO (40 nm)/QD (18 nm)/PVK (30 nm)/PEDOT:PSS (35 nm)/ZnMgO (40 nm)/QD (18 nm)/PVK (30 nm)/PEDOT:PSS (35 nm)/Al (100 nm) and ITO/ZnMgO (40 nm)/QD(18 nm)/PVK (30 nm)/PEDOT:PSS (35 nm)/ZnMgO (40 nm)/QD (18 nm)/TcTa (25 nm)/NPB(20 nm)/HATCN (10 nm)/Al (100 nm) were fabricated.

Device Fabrication: Devices were fabricated on commercially available ITO glass with a sheet resistance of 25 Ω sq^{-1}. The spin-casting processes were performed in air. Prior to deposition of functional layers, the ITO substrates were first cleaned in ultrasonic detergent for 30 min and sprayed by deionized water, followed by soaking in ultrasonic deionized water for 15 min and baking in oven for 30 min. Then the commercially obtained ZnMgO (purchased from Guangdong Poly Optoelectronics Co., Ltd.) nanoparticles were spin coated at 2500 rpm from a 30 mg mL^{-1} ethanol solution, followed by annealing at 80 °C for 15 min. The G-QD (CdZnSeS/ZnS/oleic acid, commercially obtained from Mesolight Inc. with a PL quantum yield of ≈80%) layers were spin coated from a 10 mg mL^{-1} hexane solution at 1500 rpm for 45 s and annealed at 100 °C for 5 min. The PL spectrum and TEM image of the G-QD are shown in Figure S5 (Supporting Information). After that, the PVK (10 mg mL^{-1} in chlorobenzene) hole transport layer was coated at 4000 rpm for 40 s and annealed at 80 °C for 5 min. The PEDOT:PSS solution (Clevios P VP AI 4083) doped by IPA (AR, Tianjin ZhiYuan Reagent Co. Ltd, China) with volume ratio 3:2 was spin coated at 1500 rpm for 40 s and baked at 80 °C for 5 min. The following solution-processed functional layers including ZnMgO, QDs, PVK, and PEDOT:PSS were all sequentially deposited with the same fabrication conditions as before except the annealing conditions, which were fixed at 80 °C for 5 min. After that, the samples were transferred to a high-vacuum evaporation chamber to sequentially deposit the organic materials (TcTa, NPB, and HATCN) and top Al anode at a base pressure of 5×10^{-4} Pa.

Device Characterizations: The thicknesses of all the solution-processed films were measured by a Bruker DektakXT Stylus Profiler. The depiction rates and thicknesses of evaporated organic layers and Al anode were monitored by quartz crystal microbalance. Transmittances of the ICL were measured using a 150 mm integrating sphere with a Cary 5000 UV–VIS–NIR spectrophotometer (Agilent Technologies). The cross-sectional TEM images of the tandem QLEDs were characterized via high resolution (HR)-TEM (FE-HR-TEM, JEOL-2100F), and the samples were sliced using a focused ion beam (FIB) system (Dual-Beam FIB, SEIKO SMI3050SE). The EL spectra of the devices were measured by fiber optic spectrometer (Ocean Optics USB 2000) in the normal direction. The active area of the devices was 2×2 mm^2. The EQE was measured by using a method recommended by Stephen R. Forrest.[3,42] The setup of the system and measurement steps can be referred to ref. [42] The current density–voltage–luminance (*J*–*V*–*L*) characteristics of the devices were measured by a dual-channel Keithley 2014B source measure unit and a PIN-25D silicon photodiode.

Supporting Information

Supporting Information is available from the Wiley Online Library or from the author.

Acknowledgements

This work was supported by the National Natural Science Foundation of China (61405089), the Guangdong Natural Science Funds for Distinguished Young Scholars (2016A030306017), the National Key R&D Program of China (2016YFB0401702), the Guangdong Special Support Program for Young Talent Scholar (2014TQ01X015), and the Shenzhen Peacock Plan (KQTD2015071710313656).

Keywords

all solution processing, high efficiency, interconnecting layers, quantum dot light-emitting diodes, tandem structures

Received: February 3, 2017
Revised: February 25, 2017
Published online:

[1] Y. Shirasaki, G. J. Supran, M. G. Bawendi, V. Bulovic, *Nat. Photonics* **2013**, *7*, 13.
[2] X. Dai, Z. Zhang, Y. Jin, Y. Niu, H. Cao, X. Liang, L. Chen, J. Wang, X. Peng, *Nature* **2014**, *515*, 96.
[3] B. S. Mashford, M. Stevenson, Z. Popvic, C. Hamilton, Z. Zhou, C. Breen, J. Steckel, V. Bulovic, M. Bawendi, S. Coe-Sullivan, P. T. Kazlas, *Nat. Photonics* **2013**, *7*, 407.
[4] Q. Lou, W.-Y. Ji, J.-L. Zhao, C.-X. Shan, *Nanotechnology* **2016**, *27*, 325201.
[5] J. M. Caruge, J. E. Halpert, V. Wood, V. Bulovic, M. G. Bawendi, *Nat. Photonics* **2008**, *2*, 247.
[6] W. K. Bae, Y.-S. Park, J. Lim, D. Lee, L. A. Padilha, H. McDaniel, I. Robel, C. Lee, J. M. Pietryga, V. I. Klimov, *Nat. Commun.* **2013**, *4*, 2661.
[7] W. K. Bae, J. Lim, D. Lee, M. Park, H. Lee, J. Kwak, K. Char, C. Lee, S. Lee, *Adv. Mater.* **2014**, *26*, 6387.
[8] Z. Tan, F. Zhang, J. Xu, A. Y. Wang, J. D. Dixon, L. Li, Q. Zhang, S. E. Mohney, J. Ruzyllo, *Nano Lett.* **2007**, *7*, 3803.
[9] S. He, S. Li, F. Wang, A. Y Wang, J. Lin, Z. Tan, *Nanotechnology* **2013**, *24*, 175201.
[10] D. Kim, Y. Fu, J. Kim, K. Lee, H. Kim, H. Yang, H. Chae, *Nanotechnology* **2016**, *27*, 245203.
[11] W. K. Bae, J. Kwak, J. Lim, D. Lee, M. K. Nam, K. Char, C. Lee, S. Lee, *Nano Lett.* **2010**, *10*, 2368.
[12] C.-Y. Kuei, W.-L. Tsai, B. Tong, M. Jiao, W.-K. Lee, Y. Chi, C.-C. Wu, S.-H. Liu, G.-H. Lee, P.-T. Chou, *Adv. Mater.* **2016**, *28*, 2795.
[13] K.-H. Kim, C.-K. Moon, J.-H. Lee, S.-Y. Kim, J.-J. Kim, *Adv. Mater.* **2014**, *26*, 3844.
[14] J. W. Sun, J. Y. Baek, K.-H. Kim, C.-K. Moon, J.-H. Lee, S.-K. Kwon, Y.-H. Kim, J.-J. Kim, *Chem. Mater.* **2015**, *27*, 6675.
[15] Z. Li, Y. Hu, H. Shen, Q. Lin, L. Wang, H. Wang, W. Zhao, L. S. Li, *Laser Photonics Rev.* **2017**, *11*, 1600227.
[16] H. Shen, W. Cao, N. T. Shewmon, C. Yang, L. S. Li, J. Xue, *Nano Lett.* **2015**, *15*, 1211.
[17] S. Höfle, A. Schienle, C. Bernhard, M. Bruns, U. Lemmer, A. Colsmann, *Adv. Mater.* **2014**, *26*, 5155.
[18] L.-S. Liao, W. K. Slusarek, T. K. Hatwar, M. L. Ricks, D. L. Comfort, *Adv. Mater.* **2008**, *20*, 324.
[19] H.-M. Kim, J. Lee, E. Hwang, J. Kim, J. Jang, *SID Symp. Dig. Tech. Pap.* **2016**, *47*, 1480.
[20] H. Zhang, H. Li, X. Sun, S. Chen, *ACS Appl. Mater. Interfaces* **2016**, *8*, 5493.
[21] H. Zhang, Y. Feng, S. Chen, *ACS Appl. Mater. Interfaces* **2016**, *8*, 26982.
[22] J. Kwak, W. K. Bae, D. Lee, I. Park, J. Lim, M. Park, H. Cho, H. Woo, D. Y. Yoon, K. Char, S. Lee, C. Lee, *Nano Lett.* **2012**, *12*, 2362.
[23] H. Zhang, S. Wang, X. Sun, S. Chen, *J. Mater. Chem. C* **2017**, *5*, 817.
[24] T. Chiba, Y.-J. Pu, J. Kido, *Adv. Mater.* **2015**, *27*, 4681.
[25] J.-H. Kim, C.-Y. Han, K.-H. Lee, K.-S. An, W. Song, J. Kim, M. S. Oh, Y. R. Do, H. Yang, *Chem. Mater.* **2015**, *27*, 197.
[26] H. Peng, Y. Jiang, S. Chen, *Nanoscale* **2016**, *8*, 17765.
[27] W. K. Bae, J. Kwak, J. W. Park, K. Char, C. Lee, S. Lee, *Adv. Mater.* **2009**, *21*, 1690.
[28] L. Qian, Y. Zheng, J. Xue, P. H. Holloway, *Nat. Photonics* **2011**, *5*, 543.
[29] H. Shen, Q. Lin, H. Wang, L. Qian, Y. Yang, A. Titov, J. Hyvonen, Y. Zheng, L. S. Li, *ACS Appl. Mater. Interfaces* **2013**, *5*, 12011.
[30] K.-H. Lee, J.-H. Lee, H.-D. Kang, B. Park, Y. Kwon, H. Ko, C. Lee, J. Lee, H. Yang, *ACS Nano* **2014**, *8*, 4893.
[31] Y. Yang, Y. Zheng, W. Cao, A. Titov, J. Hyvonen, J. R. Manders, J. Xue, P. H. Holloway, L. Qian, *Nat. Photonics* **2015**, *9*, 259.
[32] Y. Zou, M. Ban, W. Cui, Q. Huang, C. Wu, J. Liu, H. Wu, T. Song, B. Sun, *Adv. Funct. Mater.* **2017**, *27*, 1603325.
[33] X. Yang, K. Dev, J. Wang, E. Mutlugun, C. Dang, Y. Zhao, S. Liu, Y. Tang, S. T. Tan, X. W. Sun, H. V. Demir, *Adv. Funct. Mater.* **2014**, *24*, 5977.
[34] H.-M. Kim, J. Kim, J. Lee, J. Jang, *ACS Appl. Mater. Interfaces* **2015**, *7*, 24592.
[35] Y. Fu, D. Kim, H. Moon, H. Yang, H. Chae, *J. Mater. Chem. C* **2016**, *05*, 522.
[36] H.-H. Chou, C.-H. Cheng, *Adv. Mater.* **2010**, *22*, 2468.
[37] Y. Tao, Q. Wang, C. Yang, C. Zhong, J. Qin, D. Ma, *Adv. Funct. Mater.* **2010**, *20*, 2923.
[38] S. Watanabe, N. Ide, J. Kido, *Jpn. J. Appl. Phys.* **2007**, *46*, 3A.
[39] J. Pei, X.-L. Liu, W.-L. Yu, Y.-H. Lai, Y.-H. Niu, Y. Cao, *Macromolecules* **2002**, *35*, 7274.
[40] S. H. Kim, J. Jang, *Appl. Phys. Lett.* **2008**, *92*, 023513.
[41] S. Reineke, G. Schwartz, K. Walzer, K. Leo, *Appl. Phys. Lett.* **2007**, *91*, 123508.
[42] G. Liu, X. Zhou, S. Chen, *ACS Appl. Mater. Interfaces* **2016**, *8*, 16768.